Available online at www.sciencedirect.com
SCIENCE DIRECT®
International Journal of Pharmaceutics 298 (2005) 242–254
international journal of pharmaceutics
www.elsevier.com/locate/ijpharm

Pharmaceutical Nanotechnology

Thermal analysis of the crystallization and melting behavior of lipid matrices and lipid nanoparticles containing high amounts of lecithin

M.A. Schubert, B.C. Schicke, C.C. Müller-Goymann *

Institut für Pharmazeutische Technologie, Technische Universität, Braunschweig, Mendelssohnstraße 1, D-38106 Braunschweig, Germany

Received 6 October 2004; received in revised form 10 March 2005; accepted 14 April 2005
Available online 17 May 2005

Abstract

Lipid nanoparticles (LNP) based on triglycerides containing high amounts of the amphiphilic lipid lecithin have been proposed as a promising alternative drug delivery system with regard to drug loading capacity. Aim of the present study is to evaluate the influence of lecithin within the lipid matrix (LM) on the crystallization behavior by thermoanalysis and wide angle X-ray diffraction (WAXD). The crystallinity of LM and LNP is mainly determined by the triglyceride content. However, lecithin influences the crystallization behavior significantly. WAXD shows an accelerated polymorphic transition of the LM to the β-modification upon storage with increasing lecithin content. Both, the melting point and the crystallization temperature are not affected by the lecithin concentration and are comparable to recrystallized triglyceride bulk. However, the crystallinity indices (CI) of LM show a general decrease by 10% suggesting an incomplete crystallization. For the formation of LNP at least 10% lecithin is necessary and all systems are present in the stable β-modification. In comparison to the undispersed LM, the crystallization temperature of LNP is significantly decreased by about 20 °C whereas the melting point is reduced by about 5 °C only. Melting enthalpy is comparable to the untreated triglyceride bulk and elevated in comparison to the undispersed LM. Isothermal heat-conduction microcalorimetry (IMC) enables the determination of crystallization kinetics after fitting of the heat flow volume according to the Avrami equation.

Keywords: Crystallization; Lipid nanoparticles; Thermal analysis; X-ray diffraction

1. Introduction

The sustained release of drugs from solid lipid matrices is known in pharmacy for many years, e.g. drug release from lipid pellets. Based on this knowledge the groups around Westesen (Siekmann and Westesen,

* Corresponding author. Tel.: +49 531 3915650; fax: +49 531 3918108.
E-mail address: c.mueller-goymann@tu-bs.de (C.C. Müller-Goymann).

0378-5173/$ – see front matter © 2005 Elsevier B.V. All rights reserved.
doi:10.1016/j.ijpharm.2005.04.014

1992) and Müller (Müller and Lucks, 1996) developed in the early nineties solid lipid nanoparticles (SLN) to overcome burst release and drug leakage from nanoemulsions. SLN are in the submicron size range and consist of physiological lipids predominately triglycerides. The standard production method for SLN preparation is melt-emulsification preferably by high pressure homogenization avoiding organic solvent and allowing large scale production. So far, a wide variety of drugs such as retinol, prednisolone, doxorubicin, etc. have been successfully incorporated into SLN (Cavalli et al., 1993; Mehnert et al., 1997; Jenning et al., 2000a). However, for most drugs the payload is low because of the crystalline structure of the lipid matrices and drug expulsion is observed upon storage (Westesen et al., 1997a). Drug expulsion is attributed to a reduction of amorphous regions in the carrier lattice due to polymorphic transitions (Jenning et al., 2000b).

Triglycerides, the matrix constituent of most SLN, show a complex polymorphic behavior and can crystallize in three basic polymorphic forms termed alpha (α), beta prime (β′) and beta (β). Polymorphic transformations are monotropic and take place from α to β′ to β, the last one being the thermodynamically stable polymorph. In addition, most triglycerides especially complex triglyceride mixtures like suppository bases exhibit an intermediate crystal form (β_i) that is located between β′ and β (Larsson, 1966; Hagemann, 1988). According to Siekmann and Westesen (1994) and Bunjes et al. (1996) the melting and crystallization properties of colloidally dispersed triglycerides differ significantly from those of their bulk materials. Concerning the final product, particle solidification and crystallization after melt homogenization must be ensured to obtain a sustained drug release and stable product. Recently, nanosuspensions based on solidified reverse micellar solutions (SRMS) offering higher drug loading capacities compared to conventional triglyceride matrices have been proposed as an alternative drug delivery system (Friedrich and Müller-Goymann, 2003).

The objective of this work is to consider the effects of phospholipid incorporation within the triglyceride matrix on the melting and crystallization behavior of both lipid matrices and lipid nanoparticles and to observe and analyze the crystallization process time-dependently. Isothermal heat-conduction microcalorimetry (IMC) as a tool for the in situ observation of the crystallization process was employed and compared to differential scanning calorimetry and X-ray diffraction in order to establish IMC as an additional method for the observation and analysis of crystallization processes.

2. Materials and methods

2.1. Materials

Softisan® 154 (S154), also called “hydrogenated palm oil”, was a gift from CONDEA (Witten, Germany). It is a triglyceride mixture of natural, hydrated, even chained and unbranched fatty acids, about 97% are palmitic and stearic acid, with a melting point of circa 55–60 °C. Phospholipon® 90 G (P90G) provided by Phospholipid (Köln, Germany) is a purified, deolied, and granulated soy lecithin with a phosphatidylcholine content of at least 90%. Thimerosal was purchased from Sigma–Aldrich (Seelze, Germany). Solutol® HS15 (SOL), a nonionic solubilizer for injection solutions consisting of polyglycol mono- and diesters of 12-hydroxystearic acid and of about 30% of free polyethylene glycol, was supplied by BASF (Ludwigshafen, Germany). Water was used in bidistilled quality.

2.2. Preparation of lipid matrices (LM)

S154 and P90G were weighted into sealed containers. The ratio of P90G in the binary mixture was varied between 0% and 50% (w/w). The mixtures were stirred with a Teflon coated magnet at 70 °C until a transparent yellow solution was obtained. The solution was stirred at room temperature until solidification.

2.3. Preparation of lipid nanoparticles (LNP)

The basic formulation, if not mentioned otherwise, is composed of 15% LM, 3% Solutol® HS15 (SOL) and 82% of an 0.005% thimerosal solution in bidistilled water (all w/w). All components were weighted into sealed containers and heated up to 70 °C. Then hot preemulsions were produced by using an Ultra Turrax® (Ika, Staufen, Germany) at 13,000 rpm for 5 min. The hot preemulsions were homogenized at a pressure of 1000 bar and a temperature of about 50 °C with an EmulsiFlex®-C5 (Avestin, Ottawa, Canada) high pressure homogenizer for 20 cycles. Afterwards the dis-

persions were allowed to recrystallize subsequently at room temperature (Müller and Lucks, 1996). LNP are named according to the lecithin content of the respective LM indicating in brackets the lecithin ratio of the respective LM, e.g. LNP(20) if LM(20) was used as lipid matrix.

2.4. Particle size measurement

Laser diffraction was used to determine the particle size (PS) and particle size distribution of systems with a mean particle size above 1000 nm. The measurements were performed with a Mastersizer MS 20 (Malvern, Herrenberg, Germany). Prior to measurements, about 50 mg of sample were diluted with 100 ml bidistilled water. Results were calculated with Malvern SB O9 software using the Fraunhofer approximation.

For formulations with a mean particle size smaller than 1000 nm the size distribution was investigated by photon correlation spectroscopy (PCS) using a Zetasizer 3 (Malvern, Herrenberg, Germany) modified with a He/Ne laser model 127 (Spectra Physics, Mt. View, USA). The different systems were investigated at an angle of 90° in a measuring cell AZ 10 equilibrated at 20 °C. Each sample was diluted with filtrated bidistilled water until the appropriate concentration of particles was achieved to avoid multiscattering events and measured with a sample time of 30 ms for 10 min in serial mode. Each measurement was performed in triplicate and both the particle *z*-average diameter and polydispersity index (PI) were determined.

2.5. Differential scanning calorimetry (DSC)

Measurements were performed on a calorimeter DSC 220C connected to a disc station 5200H (Seiko, Tokyo, Japan). Approximately 10 mg of dispersion and about 3 mg of lipid matrix, respectively, were accurately weighted into an aluminum crucible, which were hermetically sealed and then measured against an empty reference crucible. Heating curves were recorded with a scan rate of 5 °C/min from 20 °C to 85 °C. For analysis of the recrystallization process samples were heated up to 85 °C as described before, kept 15 min at 85 °C and then cooled down to 20 °C with a cooling rate of 5 °C/min.

The crystallinity index (CI) was calculated from the heat of fusion according to Eqs. (1) and (2) to determine the degree of crystallinity of lipid matrices and of LNP (Siekmann and Westesen, 1994):

$$\mathrm{CI}_{\text{lipid matrix}}\,(\%) = \frac{\text{enthalpy}_{\mathrm{LM}}\,(\mathrm{J/g})}{\text{enthalpy}_{\text{untreated S154 without lecithin}}\,(\mathrm{J/g})} \times 100 \qquad (1)$$

$$\mathrm{CI}_{\mathrm{LNP}}\,(\%) = \frac{\text{enthalpy}_{\mathrm{LNP}}\,(\mathrm{J/g})}{\text{enthalpy}_{\text{untreated S154 without lecithin}}\,(\mathrm{J/g}) \times 0.15} \times 100 \qquad (2)$$

2.6. Wide angle X-ray diffraction (WAXD)

WAXD data were taken from LM based lipid matrix. An X-ray generator PW1730/10 connected to the tube PW2213/25 (copper anode) delivered X-ray of the wavelength $\lambda = 0.1542$ nm at a high voltage of 40 kV and an anode current of 25 mA. Measurements were taken with a Goniometer PW1025/50 from 3.0° to 33.0° in a step-size of 0.015° (1 s/step) (all Philips, Eindhoven, Netherlands). The interlayer spacing *d* was determined by calculation of the diffraction peaks with the Bragg equation.

WAXD studies of LNP were performed in a Debye–Scherrer camera with a perimeter of 360 mm installed on a PW 1830 generator with a PW 2253/11 X-ray tube equipped with a copper anode and a nickel K_β filter (Philips, Kassel, Germany). Samples were filled into standard glass X-ray capillaries and the exposure time was 12 h using Agfa D7 X-ray films. The interlayer spacing was calculated from the diffraction rings using Bragg's equation.

2.7. Isothermal heat-conduction microcalorimetry (IMC)

The calorimeter used for these studies was a 2277 Thermal Activity Monitor® (TAM, Thermometric AB, Jarfalla, Sweden). Two calorimeter units were installed and run simultaneously. Two grams of the LNP dispersions and 300 mg of LM were weighed into 3 ml glass ampoules. Heat flow signals were monitored

by the Digitam Software (Thermometric AB, Jarfalla, Sweden). Measuring range for all experiments was between −1000 and 1000 μW calibrated with electrical calibration. Measuring temperature was 20 °C. Prior to the measurements, the ampoules were equilibrated for 30 min. Due to the necessary equilibration time of 30 min the total crystallization enthalpy (corresponds to heat flow over time) was not detectable and the crystallization process could not be observed from the beginning. Yet, for calculation of the crystallization kinetics the complete enthalpy of the crystallization is necessary. Therefore, both a quantification of the undetermined heat flow volume and a transformation of heat flow volume in consideration of the undetermined heat flow volume fraction and the equilibration time was necessary. For that purpose the theoretical crystallization enthalpy ($\Delta H_{\text{Theor.}}$) of each LNP formulation was estimated using the melting enthalpy of untreated S154 bulk (179.3 mJ/mg measured by DSC) as reference Eq. (3):

$$\Delta H_{\text{Theor.}}\,(\text{mJ}) = 0.15 m_{\text{dispersion}}\,(\text{mg}) \times \text{fraction of S154 in LM} \times 179.3\,\text{mJ/mg} \quad (3)$$

Then the IMC measured enthalpy (ΔH_{IMC}) was determined by integration of the heat flow over time, and the ratio $R_{\Delta H}$ of ΔH_{IMC} to $\Delta H_{\text{Theor.}}$ was calculated Eq. (4):

$$R_{\Delta H} = \frac{\Delta H_{\text{IMC}}}{\Delta H_{\text{Theor.}}} \quad (4)$$

$R_{\Delta H}$ corresponds to IMC determined enthalpy fraction whereas $1 - R_{\Delta H}$ corresponds to the undetermined enthalpy fraction. Isothermal crystallization kinetics are described by the Avrami equation Eq. (5) (Avrami, 1939; Avrami, 1940):

$$x(t) = 1 - \mathrm{e}^{-kt^n} \quad (5)$$

$x(t)$ represents the crystallized fraction at time t. The parameter k (min^{-1}) is the rate constant of isothermal crystallization. n known as the Avrami exponent is related to the type of nucleation and to the growth mechanisms of crystals particularly with regard to the directions in which growth occurs. $1 - R_{\Delta H}$ was set as $x(t_0)$ in order to take the enthalpy of the equilibration time into account. Then Avrami fits were applied to the transformed heat flow integrals.

3. Results and discussion

3.1. Characterization of the lecithin influence on LM

WAXD analysis of bulk materials (Fig. 1a) shows that lecithin possesses a prominent peak at 1.2 nm ($2\theta = 7.5°$) whereas untreated bulk of S154 reveals three discrete peaks, at 0.38 nm ($2\theta = 23.4°$), 0.42 nm ($2\theta = 21.2°$), and 1.46 nm ($2\theta = 6.0°$) corresponding to the metastable β′-modification (Hagemann, 1988). Recrystallized S154 without lecithin (Fig. 1b–d) has two distinct WAXD peaks, at 1.6 nm ($2\theta = 5.5°$) and at 0.41 nm ($2\theta = 21.6°$), that do not change upon storage and might be presumably attributed to the α-form exhibiting a single strong interference at 0.415 nm according to (Thoma et al., 1983; Hagemann, 1988). In comparison to recrystallized S154 bulk, recrystallized LM containing at least 10% lecithin change upon storage over a period of 4 weeks significantly. One day after recrystallization LM(10) shows two peaks, at 1.6 nm ($2\theta = 5.4°$) and 0.41 nm ($2\theta = 21.5°$), being comparable to recrystallized S154. Four weeks later (Fig. 1d) four characteristic peaks, at 1.43 nm ($2\theta = 6.2°$), 0.46 nm ($2\theta = 19.5°$), 0.42 nm ($2\theta = 21.3°$) and 0.38 nm ($2\theta = 23.4°$), are detected. WAXD data suggest that LM(10) are present in the β as well as in the β′-modification after storage. A similar behavior is observed for LM containing more lecithin (Fig. 1b–d). Yet, the polymorphic transition from β′- to β-modification seems to occur faster; already 1 day after recrystallization both the β′-form and β-form can be detected for LM(30). In addition peak intensities decrease with increasing lecithin content indicating a loss in LM crystallinity probably caused by the reduced triglyceride content in the lipid matrices. The characteristic lecithin interference at 1.2 nm ($2\theta = 7.5°$) was detected for LM(30) 1 week after preparation and for LM(50) already 1 day after recrystallization pointing at lecithin association and orientation in distinct units in the lipid matrices.

Time-resolved WAXD was performed to analyze the crystallization process especially of the LM with higher lecithin content in more detail. Fig. 1e

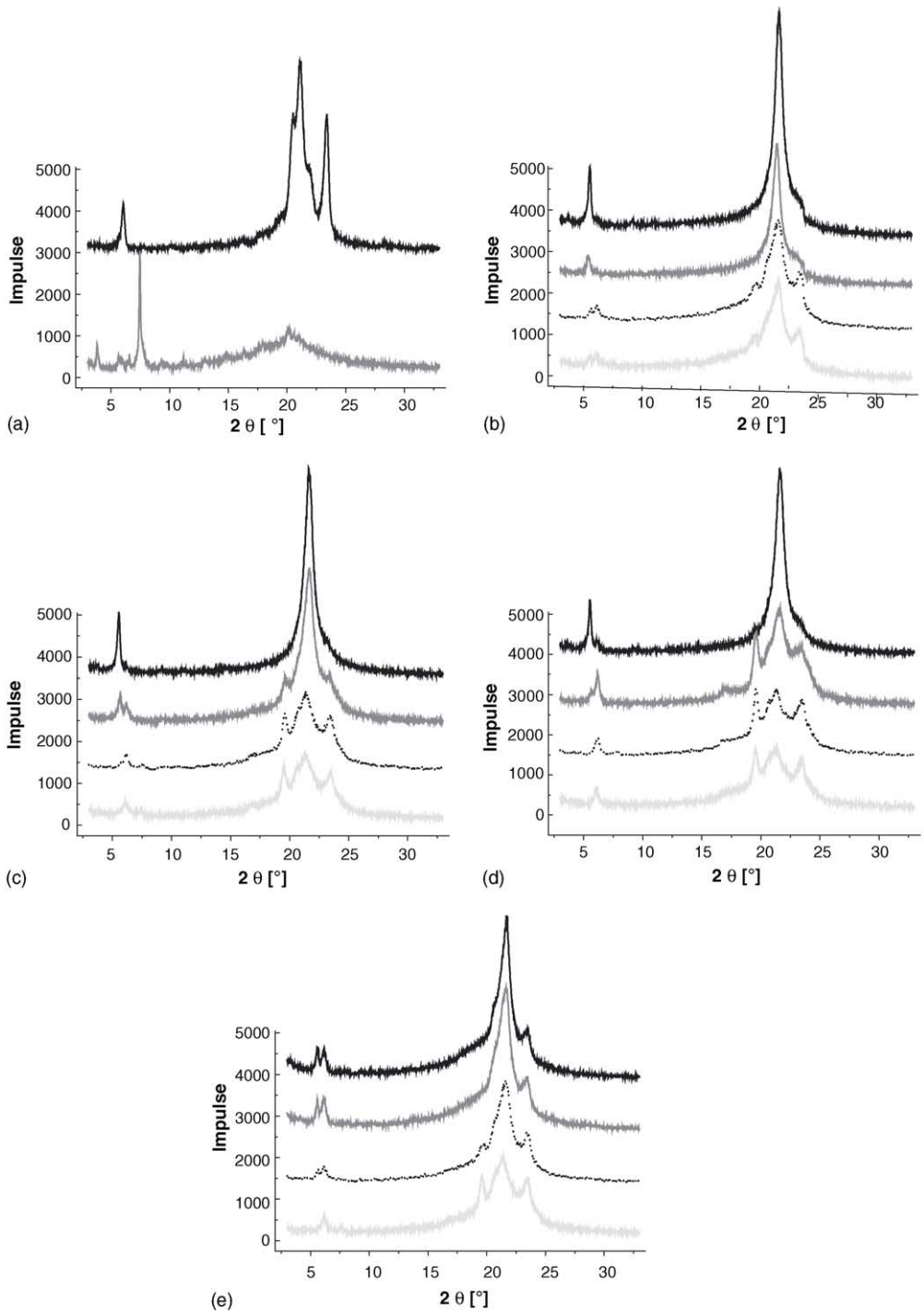

Fig. 1. WAXD analysis of the crystallization process of LM: (a) untreated bulk: S154 = black line, lecithin = gray line; (b) 1 day after crystallization: S154 = black line, LM(10) = dark gray line, LM(30) = dotted line, LM(50) = light gray line; (c) 7 days after crystallization: S154 = black line, LM(10) = dark gray line, LM(30) = dotted line, LM(50) = light gray line; (d) 4 weeks after crystallization: S154 = black line, LM(10) = dark gray line, LM(30) = dotted line, LM(50) = light gray line; (e) LM(30) crystallization vs. time: 0.5 h = black line, 12 h = dark gray line, 24 h = dotted line, 7 days = light gray line.

Table 1
Crystallization behavior of lipid matrices and LNP with varying lecithin content: crystallization index (CI) ± standard deviation and $T_{solidification}$ ± standard deviation, $n = 3$

Matrix	Lipid matrix		Lipid nanoparticles	
	CI (%)	$T_{solidification}$ (°C)	CI (%)	$T_{solidification}$ (°C)
S154	−71.3 ± 1.0	43.1 ± 0.1	–	–
LM(10)	−65.8 ± 2.4	42.7 ± 0.6	−69.7 ± 3.2	23.1 ± 0.7
LM(20)	−58.0 ± 1.5	42.8 ± 0.5	−60.0 ± 3.7	22.4 ± 0.4
LM(30)	−51.1 ± 2.0	42.5 ± 0.4	−54.9 ± 4.3	22.7 ± 0.3
LM(40)	−44.6 ± 1.2	42.9 ± 0.8	−46.1 ± 1.7	23.4 ± 0.8
LM(50)	−37.4 ± 1.9	42.4 ± 0.6	−36.0 ± 1.6	23.1 ± 0.4
Linear fit of				
CI	$y = -0.68x - 3.97$		$y = -0.83x - 4.96$	
R	0.999		0.996	

shows that 30 min after solidification of LM(30) two prominent peaks, at 0.41 nm ($2\theta = 21.6°$) and 0.38 nm ($2\theta = 23.5°$), are present changing not significantly over 12 h and indicating the presence of the α- and the β′-modification. 24 h after solidification, the interference pattern has changed, by now an additional peak has occurred at 0.46 nm ($2\theta = 19.5°$) and the strongest interference has shifted slightly from 0.41 nm ($2\theta = 21.6°$) to 0.42 nm ($2\theta = 21.4°$). During further storage signal positions do not alter in contrast to signal intensities. These findings suggest that after 24 h the α-form has completely transformed to the β′- and the β-polymorph. During storage the β′-form is converted to the β-form although the transition kinetics seem to be slow.

DSC was employed to investigate crystallization behavior as well as the melting behavior of LM. Crystallization of LM and S154 bulk (Table 1) from the previously melted material takes place at a temperature of about 43 °C and is not influenced by lecithin incorporation. The measured crystallinity depends linearly on the amount of triglyceride incorporated within the lipid matrices. In comparison to the untreated bulk an overall reduction of the CI of about 15–30% is observed with regard to the lecithin content of the lipid matrices. The strong decrease of CI can be attributed to an initial recrystallization of the triglycerides via α-modification possessing due to its fluidity a distinctly reduced crystallinity (Hagemann, 1988). Yet, the overall reduce of CI decreases with increasing lecithin content in the lipid matrix pointing at an increase in crystallization kinetics which is in agreement with former WAXD analysis.

DSC analysis of the melting behavior, displayed exemplarily for LM(30) as lipid matrix (Fig. 2), shows that directly after solidification of the lipid matrices two melting processes at about 48 °C and 57 °C can be observed. According to literature, the peak at 48 °C is attributed to the α-modification whereas the peak at 57 °C can be attributed either to the β′-, the β_i- or the β-modification (Hagemann, 1988). The enthalpy of the signal at 48 °C (Table 2, peak A) decreases continuously within the first hours after crystallization and is completely vanished after 24 h. The signal disappearance at 48 °C is accelerated for LM with a high lecithin content. Vice versa, the enthalpy of the peak minimum at 57 °C (Table 2, peak B) increases. Yet, the overall crystallinity calculated by addition of the CI of peak A and peak B remains nearly constant.

Long-time DSC measurements (Table 3) reveal that after 1 day of solidification no significant changes

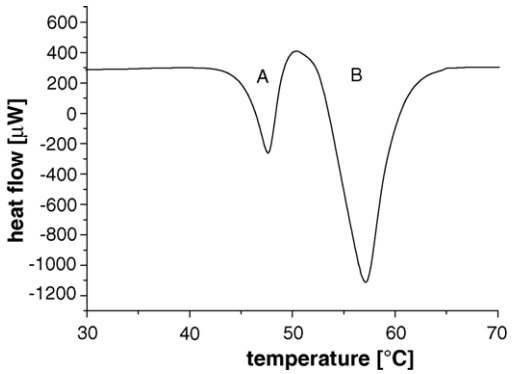

Fig. 2. DSC thermogram with melting peaks at 48 °C (peak A) and 57 °C (peak B) of LM(30), 15 min after melting.

Table 2
Analysis of the CI vs. time, lipid matrix = LM(30), $n = 1$

Time after melting (h)	CI (%) of peak A	CI (%) of peak B	CI (%) of peak A + B
0.25	14.7	47.0	61.7
0.5	12.5	50.2	62.7
5.5	7.0	56.9	63.9
10.5	3.6	60.1	63.6
20.5	0.3	64.5	64.8
25.5	0	62.0	62.0
48.0	0	60.1	60.1

Table 3
Melting behavior of LM with varying lecithin content vs. time: CI ± standard deviation and $T_{melting}$ ± standard deviation, $n = 3$

System	1 day		7 days		28 days	
	CI (%)	$T_{melting}$ (°C)	CI (%)	$T_{melting}$ (°C)	CI (%)	$T_{melting}$ (°C)
S154	89.1 ± 0.4	59.0 ± 0.2	91.8 ± 0.2	59.1 ± 0.1	91.2 ± 0.5	57.2 ± 0.1
LM(10)	80.1 ± 1.7	59.5 ± 0.6	80.3 ± 0.6	59.5 ± 0.1	81.0 ± 1.0	57.5 ± 0.1
LM(20)	70.3 ± 1.7	59.1 ± 0.4	70.2 ± 1.0	59.2 ± 0.1	73.8 ± 2.0	57.7 ± 0.6
LM(30)	62.0 ± 0.3	59.3 ± 0.5	61.6 ± 1.1	59.7 ± 0.1	64.7 ± 0.2	57.6 ± 0.6
LM(40)	50.9 ± 0.6	59.0 ± 0.3	51.6 ± 0.2	57.9 ± 0.1	52.8 ± 0.9	58.6 ± 0.1
LM(50)	42.5 ± 1.1	59.2 ± 1.1	42.1 ± 2.0	58.5 ± 0.2	43.4 ± 0.1	60.1 ± 1.0
Linear fit of						
CI	$y = 0.93x - 3.44$		$y = 1.00x - 8.63$		$y = 1.00x - 6.41$	
R	0.999		0.999		0.998	

in melting enthalpy and melting temperature are noticed. As already demonstrated for the crystallization enthalpy the melting enthalpy depends linearly on the triglyceride content as well, and the CI is about 10% reduced in comparison to untreated S154 bulk. Since the CI for solidified S154 is abased to the same extent the loss in crystallinity is due to crystallization in a less crystalline polymorph after melting and not due to a molecular incorporation of lecithin within the crystal lattice of lipid matrices. In this case a depression of melting temperature should be observed for formulations containing lecithin. But melting temperature of S154 bulk and LM is about the same and is not influenced by the lecithin incorporation. Furthermore, former WAXD data show an additional characteristic interference at 1.2 nm ($2\theta = 7.5°$) for systems containing at least 30% lecithin. This interference points to a separate lecithin crystallization besides the triglycerides.

In contrast to previous WAXD measurement, suggesting an α-form for recrystallized S154, DSC data indicate either the β′-, the β_i- or the β-form for recrystallized S154 as no decrease in CI and the melting temperature is detected.

Fig. 3 shows the IMC thermograms of S154 bulk and LM after melting. Initially the heat flow versus time shows a strong negative slope for all matrix compositions suggesting a fast crystallization of all matrices.

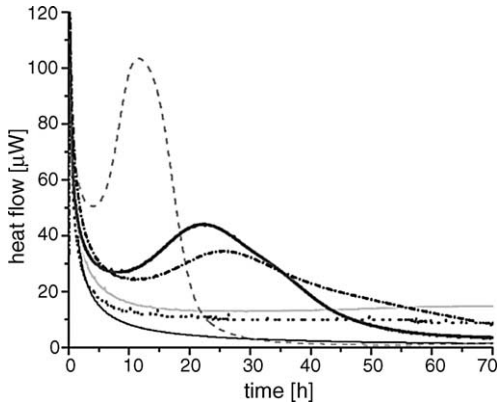

Fig. 3. Heat flow in IMC vs. time during crystallization of S154 bulk and LM with varying lecithin content, $n = 3$: S154 = thin black line, LM(10) = dotted gray line, LM(20) = gray line, LM(30) = dashed dotted black line, LM(40) = thick dark gray line, LM(50) = dashed gray line.

Table 4
Particle size (PS) ± standard deviation and polydispersity index (PI) ± standard deviation of LNP with varying lecithin content vs. time, $n = 6$

System	1 day		7 days		28 days	
	PS (nm)	PI	PS (nm)	PI	PS (nm)	PI
LNP(10)_1	12330 ± 167	–	12990 ± 1091	–	11420 ± 164	–
LNP(10)_2	275 ± 25	0.31 ± 0.08	309 ± 58	0.32 ± 0.08	275 ± 54	0.30 ± 0.08
LNP(20)	162 ± 6	0.22 ± 0.02	164 ± 2	0.20 ± 0.02	157 ± 4	0.20 ± 0.01
LNP(30)	109 ± 7	0.24 ± 0.03	101 ± 3	0.22 ± 0.02	107 ± 4	0.22 ± 0.2
LNP(40)	104 ± 5	0.20 ± 0.01	109 ± 7	0.18 ± 0.02	110 ± 1	0.21 ± 0.02
LNP(50)	120 ± 11	0.16 ± 0.03	119 ± 9	0.16 ± 0.02	130 ± 6	0.18 ± 0.03

However, further on an increase in heat flow is measured in dependence of the lecithin concentration of the matrices. LM shows a delayed increase in heat flow with decreasing lecithin content as well as a less pronounced heat flow increase. At a lecithin concentration of 10% within the matrix the heat flow increase is not detectable anymore. In addition the heat flow decline down to zero pointing at a complete crystallization process is favored by a high lecithin concentration within the matrix. We suggest that the increase in heat flow is caused by polymorphic transitions within the matrices from α to β′ to β, being in accordance with former WAXD and DSC measurements. Due to the superposing of the crystallization process by polymorphic transitions within the lipid matrices Avrami analysis of the heat flow volume was not performed.

3.2. Characterization of LNP with varying lecithin content in LM

Particle size and particle size distribution measurements were performed to ensure stability of the LNP and to exclude particle agglomeration and particle-growing-caused heat flow during IMC measurement. As can be seen in Table 4, particle sizes and particle size distributions did not change upon storage for 4 weeks. For the formation of colloidal LNP the incorporation of at least 10% lecithin within the lipid matrix is absolutely necessary. However, different batches of LM(10) show inconsistent particle sizes and no reproducible LNP production can be ensured for this matrix composition. Furthermore, the latter systems transformed into a semisolid state during storage but reliquefy either spontaneously or upon agitation; afterwards they remain liquid. The semisolid state is believed to be caused by incomplete emulsifier adsorption on the crystal interfaces (Westesen and Siekmann, 1997b). Addition of lecithin up to 30% leads to a concentration dependent particle size reduction down to 100 nm. Higher lecithin contents within the lipid matrix as to 50% were also investigated, but caused no further particle size decrease.

WAXD analysis shows that the LNP display the characteristic interference pattern of the stable β modification already 1 day after preparation. The lecithin concentration seems to influence the interference pattern only marginally (Table 5). At a lecithin concentration of 20% an additional peak appears at 0.44 nm or 0.43 nm and the interference at 0.39 nm is replaced by a broad halo reaching from 0.39 nm to 0.41 nm. These reflection patterns do not fit to any of the reported classifications of triglyceride polymorphs and have been firstly described by Bunjes et al. (2002) for very fine triglyceride nanoparticles. During storage for 28 days the interference patterns of the different formulations do not change.

Even directly after solidification LNP display only a single melting peak in DSC analysis upon heating (Fig. 5). According to DSC measurements of the different LNP, there is no change in CI and peak minimum temperature upon storage (Table 6). Furthermore, DSC data show that the CI of the crystallization of the LNP

Table 5
Interlayer spacing (nm) of LNP with varying lecithin content, peak intensities in the table are given according to following scheme: **strong** > normal > *weak* > (*very weak*), $n = 2$

LNP(10)	LNP(20)	LNP(30)	LNP(40)	LNP(50)
0.53	*0.53*	(*0.53*)	(*0.53*)	(*0.53*)
0.46	**0.46**	**0.46**	**0.46**	**0.46**
–	0.44	0.44	0.43	0.43
0.39	0.41–0.39	0.41–0.39	0.41–0.39	0.41–0.39
0.37	**0.37**	**0.37**	**0.37**	**0.37**

Table 6
Melting behavior of LNP with varying lecithin content vs. time: CI ± standard deviation and $T_{melting}$ ± standard deviation, $n = 6$

System	1 day		7 days		28 days	
	CI (%)	$T_{melting}$ (°C)	CI (%)	$T_{melting}$ (°C)	CI (%)	$T_{melting}$ (°C)
LM(10)	91.2 ± 2.6	55.6 ± 1.5	95.2 ± 4.5	56.5 ± 0.3	91.5 ± 1.6	56.5 ± 0.2
LM(20)	83.9 ± 1.6	52.7 ± 0.2	83.2 ± 2.1	52.8 ± 0.1	81.8 ± 2.0	52.3 ± 0.2
LM(30)	68.0 ± 1.1	52.5 ± 0.2	67.0 ± 1.0	52.3 ± 0.2	68.0 ± 2.4	52.4 ± 0.1
LM(40)	56.2 ± 2.0	54.1 ± 0.8	60.0 ± 2.2	55.0 ± 0.1	58.8 ± 3.5	55.2 ± 0.1
LM(50)	44.6 ± 2.1	54.3 ± 0.2	45.5 ± 1.4	54.3 ± 0.1	46.0 ± 1.1	55.2 ± 0.1
Linear fit of						
CI	$y = -0.01x + 1.05$		$y = -0.01x + 1.07$		$y = -0.01x + 1.03$	
R	0.996		0.995		0.998	

(Table 1) as well as the melting of the LNP (Table 6) depend linearly on the triglyceride amount in the different matrices (Fig. 4) being in accordance with former measurements of bulk LM. In comparison to undispersed LM (Table 3) the CI of dispersed LM is about 10% elevated reflecting an LNP crystallization directly in the more stable β-form which is supported by former WAXD analysis. However, it has to be considered that for the calculation of the CI only the melting enthalpy is taken into account (see Eqs. (1) and (2)) so that despite a comparable CI of LNP and untreated triglyceride bulk the CI of a β- and a β′-polymorph are compared. The absence of a detectable α-form in WAXD and DSC analysis suggests faster polymorphic transition kinetics for LNP compared to LM bulk. In addition the increase of CI in the dispersed LM in comparison to undispersed LM may hint at a different lecithin distribution in dispersed and undispersed systems.

The melting temperature of LNP shows a reduction of only about 5 °C compared to S154 bulk. Contrarily to the LNP melting temperature, the LNP crystallization temperature at about 23 °C differs distinctly from the undispersed matrices (Fig. 5). This finding suggests storage below 23 °C is necessary in order to ensure complete triglyceride crystallization within the LNP. Since S154 is a triglyceride mixture of long fatty acid chains with a rather high melting point, hard fats with lower melting points and shorter fatty acid chains may have to be stored refrigerated in order to ensure crystallization of the solid lipid after melt homogenization. This may be a possible explanation for controversial reports describing the crystalline state of solid lipid nanoparticles (Westesen and Bunjes, 1995).

In Fig. 6 the heat flow of LNP crystallization is shown versus time. The heat flow signal depends on the lipid matrix composition. A high amount of P90G in

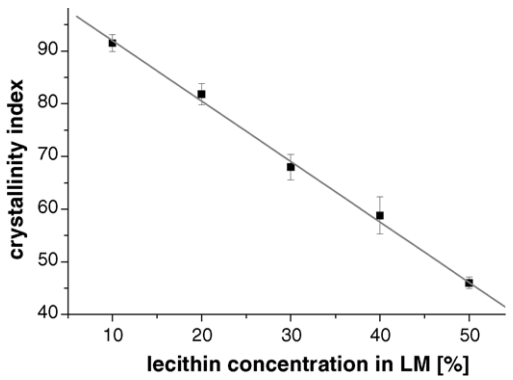

Fig. 4. CI (black squares) ± standard deviation (bars) of LNP with varying lecithin content after a storage time of 28 days, linear fit (gray line): $y = -0.01x + 1.03$, $R = 0.998$, $n = 6$.

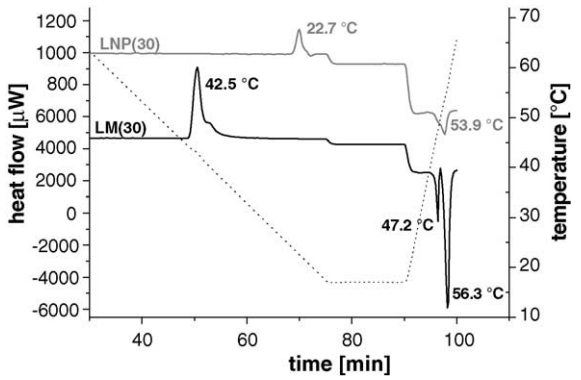

Fig. 5. DSC analysis of the recrystallization behavior of LNP(30) (gray line) and LM(30) (black line), temperature during measurement (dotted black line).

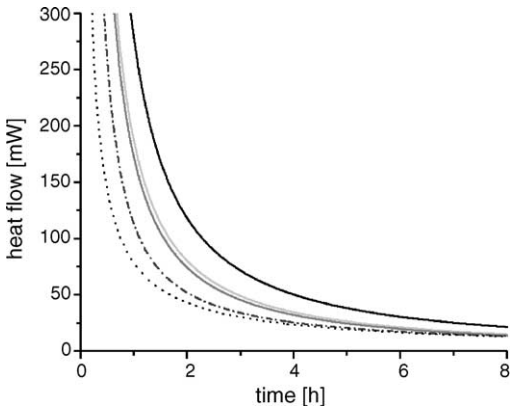

Fig. 6. Heat flow in IMC vs. time during crystallization of LNP with varying lecithin content, $n = 4$: LNP(10) = black line, LNP(20) = light gray line, LNP(30) = dark gray line, LNP(40) = dashed dotted gray line, LNP(50) = dotted black line.

the matrix causes a decreased heat flow signal, because the crystallization occurs mainly between triglycerides. Lecithin itself shows no crystalline structure at solidification and therefore systems with a high lecithin content show a reduced heat flow signal. Integration of the heat flow versus time and determination of $\Delta H_{\text{Theor.}}$, allows the calculation of $R_{\Delta H}$ (Table 7) corresponding to the measured fraction of crystallization enthalpy. $R_{\Delta H}$ is for all matrix modified LNP about 0.2, i.e. the main fraction of crystallization enthalpy, about 80%, was not measured by IMC. Thus, the equilibration time of 30 min being necessary to ensure isothermal crystallization conditions in IMC allows only detection of the last part of crystallization growth phase whereas the nucleation phase in which the seed crystals are formed is not detectable. Despite different curve progressions in IMC similar $R_{\Delta H}$ suggest an equal effective crystallization velocity for the different compositions. Yet, curve fitting after transformation according to the Avrami equation shows that the velocity profile of crystallization expressed by the Avrami exponents n and k (Table 7) differs for the different compositions in dependence of the lecithin content in the lipid matrix. The Avrami exponent n decreases from 0.59 to 0.42 with increasing lecithin content in the LNP matrix. In contrast, the Avrami factor k increases from 1.53 to 3.63 (min^{-1}) with increasing lecithin content in LNP matrix. The value of n of about 0.5 indicates a site saturated diffusion controlled crystal growth in nearly one dimension (Hulbert, 1969; Asencio et al., 2002; Latsch et al., 2004). Vanhoutte et al. (2002) observed that crystallization of anhydrous milk fat was delayed at high phospholipid concentrations and assumed that the delay in crystallization was caused by adsorption of phospholipids on the growth sites of the crystals. This scenario might be an explanation for the observed decrease in Avrami exponent n with rising lecithin content. Vice versa, the growth rate parameter k increases with increasing lecithin content in LNP matrix, and compensates for the decrease in Avrami exponent n, so that the overall crystallization rate is nearly the same for all systems.

Table 7
$R_{\Delta H}$ and Avrami parameters n and k of LNP with varying lecithin content

System	$R_{\Delta H}$	n	k (min^{-1})
LNP(10)	0.20	0.59	1.53
LNP(20)	0.20	0.51	2.19
LNP(30)	0.21	0.53	2.03
LNP(40)	0.21	0.45	2.96
LNP(50)	0.22	0.42	3.63

3.3. Characterization of LNP with varying nonionic emulsifier concentration

To detect the influence of non ionic emulsifier on the crystallization behavior of the LNP, systems containing a constant lecithin concentration of 30% were produced under variation of the emulsifier concentration in the range of 1.5% and 7.5%. Measurements with PCS show a constant particle size and particle size distribution for each emulsifier concentration during 28 days of storage (Table 8). With increasing emulsifier concentration particle size decreases from 300 nm down to 70 nm, simultaneously the particle size distribution expressed by the polydispersity index is reduced. The DSC thermograms do not change during storage in terms of the melting temperature and the melting enthalpy for the respective emulsifier concentrations (Fig. 7) but are changing in dependence of emulsifier concentration. LNP with a particle size of about 65 nm corresponding to an emulsifier to lipid ratio of 1:2 have a melting temperature of about 50 °C and CI of 70%. With increasing particle size the melting temperature is elevated up to about 57 °C and the CI increases up to 76%. The decrease in crystallinity with decreasing particle size is related to the colloidal dimensions of the particles in particular to

Table 8
Particle size analysis of LNP(30) with varying emulsifier (SOL) concentration vs. time: particle size (PS) ± standard deviation and polydispersity index (PI) ± standard deviation, $n = 3$

SOL (%)	1 day		7 days		28 days	
	PS (nm)	PI	PS (nm)	PI	PS (nm)	PI
1.5	325 ± 13	0.28 ± 0.02	317 ± 6	0.22 ± 0.01	300 ± 14	0.25 ± 0.03
3.0	100 ± 1	0.19 ± 0.02	95 ± 4	0.17 ± 0.02	103 ± 2	0.22 ± 0.01
7.5	61 ± 1	0.17 ± 0.02	64 ± 3	0.15 ± 0.03	69 ± 3	0.21 ± 0.04

an increase of the surface to volume ratio and is not related to crystallization in an α-modification (Siekmann and Westesen, 1994). This assumption is supported by WAXD data showing that all formulations exist in the stable β-modification (data not shown because diffraction patterns of the different LM(30) formulations are in accordance with data given in Table 5).

Despite similar LNP matrix composition and therewith similar triglyceride contents, thermal analysis with IMC (Fig. 8) reveals different heat flow profiles with different emulsifier concentrations suggesting an influence of the particle size on crystallization kinetics. LNP with the highest emulsifier concentration in the aqueous phase show the lowest heat flow as well as the fastest descend of the heat flow towards zero suggesting the fastest crystallization process. With decreasing emulsifier concentration in the formulations a more pronounced heat flow at elevated levels is observed for

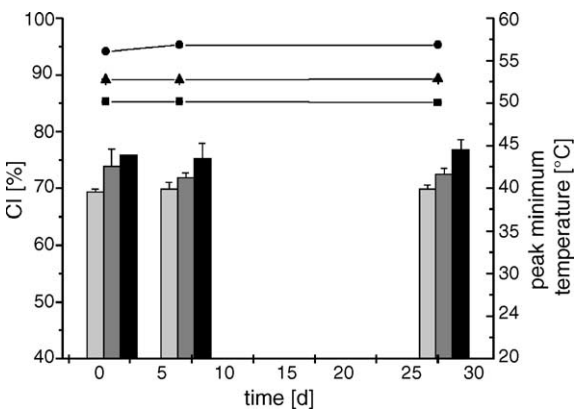

Fig. 7. Columns + bars: CI + standard deviation of LNP(30) with varying emulsifier content (SOL) vs. storage time, $n = 3$: 7.5% SOL = light gray bar, 3.0% SOL = dark gray bar, 1.5% SOL = black bar. Symbols ± bars: melting temperature ± standard deviation of LNP(30) with varying SOL content vs. storage time, $n = 3$: 7.5% SOL = squares, 3.0% SOL = triangles, 1.5% SOL = circles.

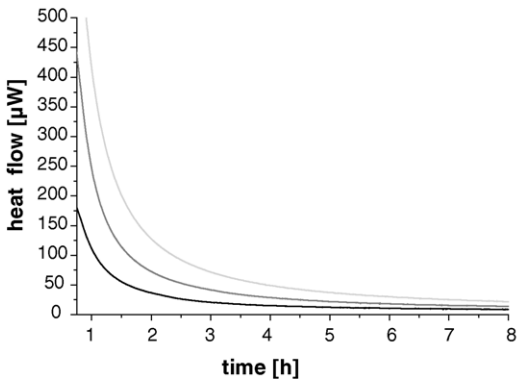

Fig. 8. Heat flow in IMC during crystallization of LNP(30) with varying emulsifier (SOL) content, $n = 3$: 1.5% SOL = light gray line, 3:0% SOL = dark gray line, 7.5% SOL = black line.

a longer time. Determination of $R_{\Delta H}$ for the different emulsifier concentrations supports this assumption showing an increase of $R_{\Delta H}$ from 0.11 to 0.40 (Table 9) with decreasing emulsifier concentration. The Avrami parameter n (Table 9) of the emulsifier modified LNP is again around 0.5 and points to a site saturated diffusion controlled crystal growth. While the Avrami parameter n changes only slightly for the different formulations the Avrami exponent k increases from about 0.9 to 7.6 min^{-1} with increasing emulsifier concentration indicating a fast crystal growth (Table 9). This finding is in agreement with previous data interpretation of IMC heat flow as well as $R_{\Delta H}$. Linear regression with a correlation coefficient R of 0.924 reveals a linear relationship

Table 9
$R_{\Delta H}$ and Avrami parameters n and k of LNP(30) with varying emulsifier (SOL) concentration

SOL (%)	$R_{\Delta H}$	n	k (min^{-1})
1.5	0.40	0.63	0.89
3.0	0.24	0.49	2.00
7.5	0.11	0.37	7.57

between the particle surface and the crystal growth parameter *k*. A possible explanation for this phenomenon may be that the heat transfer is mainly governed by the surface area provided by the particles. IMC analysis of the Avrami exponent *k* supports the assumption that the decrease in crystallinity and melting temperature which was measured by DSC has to be attributed only to the colloidal dimensions of the systems.

4. Conclusion

The crystallinity of LM as well as of LNP is only governed by triglyceride concentration within the systems. Yet, lecithin incorporation influences the crystallization behavior of dispersed and undispersed systems significantly. WAXD data show that LM shows an accelerated polymorphic transition to the stable β-modification with increasing lecithin content. However, kinetics of polymorphic transition are so slow that the transition is still incomplete after 4 weeks and thus both the β′- and β-modification are detected in all systems. The polymorphic transition of LM bulk could also be detected with DSC and IMC showing polymorphic transitions particularly in the first hours of crystallization. Both, the melting point and the crystallization temperature are not influenced by the lecithin concentration and are comparable to recrystallized S154 bulk. However, the CI of recrystallized S154 and LM with regard to the lecithin content shows a general decrease of 10% suggesting an incomplete crystallization.

For the formation of LNP at least 10% lecithin is necessary. All systems are present in the stable β-modification, however at a lecithin content of 20% additional interferences appear that cannot attributed to any known polymorph. The melting point is not influenced by the lecithin content and is reduced about 5 °C in comparison to untreated bulk. Melting enthalpy is comparable to the untreated S154 and elevated in comparison to the undispersed systems. Furthermore, LNP show a significant decrease of about 20 °C in the crystallization temperature.

IMC is an appropriate method for in situ observation of the crystallization behavior and kinetics of LNP and LM provided other methods such as X-ray diffraction and DSC are consulted to assure correct assignment of polymorphic modifications. Due to the essential equilibration time IMC is particularly suitable for slow procedures as has been shown for the polymorphic transitions of LM. Due to its high sensitivity IMC can also be applied to ongoing processes on the basis of recording heatflow segments at given time intervals to yield extrapolated data usually performed in stability tests (Beezer et al., 1999). Provided that the reaction mechanism is known IMC allows for the calculation of kinetic such as recrystallisation kinetics for example.

Acknowledgements

We like to thank BASF, Condea and Phospholipid for kind support with materials.

References

Asencio, I., Dorado, F., Sánchez, P., Lobato, J., 2002. Calculation of kinetic parameters for crystallization processes. The Chemical Educator, abstract volume 7, pp. 19–22, doi:10.1333/s00897010527a.

Avrami, M., 1939. Kinetics of phase change: I. General theory. J. Chem. Phys. 7, 1103–1112.

Avrami, M., 1940. Kinetics of phase change: II. Transformation-time relations for random distribution of nuclei. J. Chem. Phys. 8, 212–224.

Beezer, A.E., Gaisford, S., Hills, A.K., Willson, R.J., Mitchell, J.C., 1999. Pharmaceutical microcalorimetry: applications to long-term stability studies. Int. J. Pharm. 179, 159–165.

Bunjes, H., Westesen, K., Koch, M.H.J., 1996. Crystallization tendency and polymorphic transitions in triglyceride nanoparticles. Int. J. Pharm. 129, 159–173.

Bunjes, H., Koch, M.H.J., Westesen, K., 2002. Effect of particle size on colloidal solid triglycerides. Langmuir 16, 5234–5241.

Cavalli, R., Caputo, O., Gasco, M.R., 1993. Solid lipospheres of doxorubicin and idarubicin. Int. J. Pharm. 89, R9–R12.

Friedrich, I., Müller-Goymann, C.C., 2003. Characterization of solidified reverse micellar solutions (SRMS) and production development of SRMS-based nanosuspensions. Eur. J. Pharm. Biopharm. 56, 111–119.

Hagemann, J.W., 1988. Thermal behaviour and polymorphism of acylglycerides. In: Garti, N., Sato, K. (Eds.), Crystallization and Polymorphism of Fats and Fatty Acids. Marcel Dekker, New York, USA, pp. 29–67.

Hulbert, S.F., 1969. Models for solid-state reactions in powdered compacts: a review. J. Br. Ceram. Soc. 6, 11–20.

Jenning, V., Gysler, A., Schäfer-Korting, M., Gohla, S.H., 2000a. Vitamin A loaded solid lipid nanoparticles for topical use: occlusive properties and drug targeting to the upper skin. Eur. J. Pharm. Biopharm. 49, 211–218.

Jenning, V., Schäfer-Korting, M., Gohla, S.H., 2000b. Vitamin A loaded solid lipid nanoparticles for topical application: drug release properties. J. Control. Rel. 66, 115–126.

Larsson, K., 1966. Classification of glyceride crystal forms. Acta Chem. Scand. 20, 2255–2260.

Latsch, S., Selzer, T., Fink, L., Kreuter, J., 2004. Determination of the physical state of norethindrone acetate containing transdermal drug delivery systems by isothermal microcalorimetry, X-ray diffraction, and optical microscopy. Eur. J. Pharm. Biopharm. 57, 383–395.

Mehnert, W., zur Mühlen, A., Dingler, A., Weyhers, H., Müller, R.H., 1997. Solid Lipid Nanoparticles—ein neuartiger Wirkstoff-Carrier für Kosmetika und Pharmazeutika, 2. Mitt.: Wirkstoff-Inkorporation, Freisetzung und Sterilisierbarkeit. Pharm. Ind. 59, 511–514.

Müller, R.H., Lucks, S., 1996. Arzneistoffträger aus festen Lipidteilchen (feste Lipidnanosphären) (SLN)). European Patent 0605497.

Siekmann, B., Westesen, K., 1992. Sub-micron sized parenteral carrier systems based on solid lipid. Pharm. Pharmacol. Lett. 1, 123–126.

Siekmann, B., Westesen, K., 1994. Thermoanalysis of the recrystallization process of melt-homogenized glyceride nanoparticles. Colloids Surf. B 3, 159–175.

Thoma, K., Serno, P., Precht, D., 1983. Röntgendiffraktometrischer Nachweis der Polymorphie von Hartfett. Pharm. Ind. 45, 420–425.

Vanhoutte, B., Foubert, I., Duplacie, F., Huyghebaert, A., Dewettinck, K., 2002. Effect of phospholipids on isothermal crystallization and fractionation of milk fat. Eur. J. Lipid Sci. Technol. 104, 738–744.

Westesen, K., Bunjes, H., 1995. Do nanoparticles prepared from lipids solid at room temperature always possess a solid lipid matrix? Int. J. Pharm. 115, 129–131.

Westesen, K., Bunjes, H., Koch, M.H.J., 1997a. Physicochemical characterization of lipid nanoparticles and evaluation of their drug loading capacity and sustained release potential. J. Control. Rel. 48, 223–236.

Westesen, K., Siekmann, B., 1997b. Investigations of the gel formation of phospholipid-stabilizided solid lipid nanoparticles. Int. J. Pharm. 151, 35–45.